Versatile microfluidic flow generated by moulded magnetic artificial cilia

Versatile microfluidic flow generated by moulded magnetic artificial cilia†

Shuaizhong Zhang (张帅重),[ab] Ye Wang,[ab] Reinoud Lavrijsen,[c] Patrick R. Onck[d] and Jaap M.J. den Toonder*[ab]

[a] Department of Mechanical Engineering, Eindhoven University of Technology (TU/e), P.O. Box 513, 5600 MB Eindhoven, The Netherlands. E-mail: J.M.J.d.Toonder@tue.nl
[b] Institute for Complex Molecular Systems, ICMS, De Zaale, 5612 AJ Eindhoven, The Netherlands
[c] Department of Applied Physics, Eindhoven University of Technology, P.O. Box 513, 5600 MB Eindhoven, The Netherlands
[d] Zernike Institute for Advanced Materials, University of Groningen, Groningen, The Netherlands.
† Electronic Supplementary Information (ESI) available.

Magnetic artificial cilia (MAC) are flexible hair-like micro-actuators inspired by biological cilia. When integrated in a microfluidic device and actuated by an external (electro-)magnet, MAC can generate fluid flows. Our MAC are made of a composite material of polydimethylsiloxane (PDMS) and magnetic microparticles (Carbonyl iron powder). In this paper, we demonstrate a fabrication process based on micro-moulding to manufacture MAC, in which we can vary the magnetic particle distribution within the cilia from (1) a random distribution, to (2) a linearly aligned distribution to (3) a concentrated distribution in the tips of the cilia. Magnetization measurements show that the aligned distribution leads to a substantial increase of magnetic susceptibility, which dramatically enhances their response to an applied magnetic field. When integrated in a microfluidic channel, the improved MAC can induce versatile flows, for example (i) circulatory fluid flows with flow speeds up to 250 µm/s which is substantially above the performance of most of the previously developed artificial cilia, (ii) direction-reversible flows, (iii) oscillating flows, and (iv) pulsatile flows, by changing the magnetic actuation mode. Compared to other pumping methods, this on-chip / in-situ micro-pump requires no tubing or electric connections, reducing the usage of reagents by minimizing "dead volumes", avoiding undesirable electrical effects, and accommodating a wide range of different fluids. These results demonstrate that our MAC can be used as versatile integrated micropump in microfluidic devices, with great potential for future lab-on-a-chip applications.

Keywords: Magnetic artificial cilia; Micro-pump; Versatile microfluidic flow; Micro-moulding; Magnetic particle distribution; Lab-on-Chip

1. Introduction

Microfluidics is the science and technology of systems that manipulate fluids at small scales (typically from 10^{-4} to 10^{-8} liters) for applications such as chemical synthesis and biological analysis [1]. In this field, (micro-)pumping is a paramount function. Nowadays, most adopted approaches either need large peripherals, such as pneumatic control systems or syringe pumps, or they are expensive and/or cumbersome to integrate. To address these issues, researchers have sought inspiration from nature to create truly integrated microfluidic pumps by mimicking the functionality of biological cilia. Biological cilia are micro-hairs with a typical length between 2 and 15 µm, which are found ubiquitously in nature [2]. By moving in a coordinated, asymmetric manner, cilia are very effective in generating flows in a low Reynolds number environment where inertial effects are negligible and the flow is dominated by viscous effects [2]. For example, the collective asymmetric motion of cilia covering the body of a paramecium propels the body forward at a speed of 10 times its body length per second.

In recent years, a number of methods and technologies have been developed to fabricate man-made analogues of biological cilia - artificial cilia - including electrostatic cilia [3], magnetic artificial cilia (MAC) [4]–[6], optically-driven cilia [7], hydrogel-actuated artificial cilia [8], resonance-actuated artificial cilia [9][10], and pneumatically actuated artificial cilia [11]. Among these, MAC are the most promising because (1) MAC can be externally actuated within microfluidic channels by permanent magnets or electromagnets without the need for physical connections to peripheral equipment, (2) MAC have an instantaneous response to the external stimulus, and (3) magnetic actuation is compatible with biological fluids.

In 2007, Evans *et al.* [12] used polycarbonate track-etched (PCTE) porous membranes as sacrificial templates to fabricate PDMS - ferrofluid based magnetic nanorod arrays with a size similar to that of natural cilia. MAC created using this technique were actuated by an offset-positioned rotating permanent magnet, such that they moved in a way mimicking the beat shape of the embryonic nodal cilia (the so-called 'tilted conical beat') [6]. This tilted conical motion of cilia was demonstrated by Downton and Stark [13] to be a simple yet effective asymmetric nonreciprocal motion to generate net fluid flows. In 2009, Vilfan *et al.* [14] exploited the self-assembling ability of magnetic colloidal micro-beads subjected to an external magnetic field, and created MAC consisting of magnetically linked chains which were anchored to electroplated nickel dots. Babataheri *et al.* [15] and Wang *et al.* [16] employed similar approaches to produce MAC with the addition of a polymer coating to achieve permanent linking between the micro-beads, so that stable chains were obtained. All the MAC mentioned above were able to produce only limited fluid flows of just several micrometers per second because of the weak magnetic response of the MAC to the applied magnetic fields. In 2014, Wang *et al.* [17] improved the self-assembly process by developing a simple and cost-effective magnetic fiber drawing method in which they used a permanent magnet to pull MAC out of a precursor layer consisting of iron micro-particles and uncured PDMS. The MAC produced in this way were able to generate a net water flow up to 70 µm/s in a closed-loop microfluidic channel. However, the method requires a large and homogenous magnetic field gradient during fabrication, which is difficult to achieve over a large surface area, limiting the practical applications of this technique.

Apart from the above-mentioned intricate and expensive approaches, in 2016, Wang *et al.* [18] developed a cost-effective, cleanroom-free, high speed and potentially large area method to produce MAC based on roll-pulling of uncured magnetic polymer precursor material, which made a step towards the implementation of artificial cilia in real-life applications. The MAC produced

in this way could generate a net fluid flow of up to 120 µm/s. However, this method still has a number of drawbacks. First, the base on which the cilia are created is magnetic as well as non-transparent. This can result in undesired magnetic interference between the MAC, the applied magnetic field, and the substrate, respectively, while optical observation is hampered. Second, the shape and size of the MAC are not easily controlled since these are limited by the physical process during the roll-pulling as well as by the rheology of the uncured precursor material. In the present paper, we address all these issues by introducing a micro-moulding technique to create slender MAC with well-defined geometries and spatial arrangements on a transparent non-magnetic substrate. Compared to most of the aforementioned methods, micro-moulding is an effective and straightforward approach. Khademolhosseini *et al.* [19] employed a similar method and successfully created MAC for cell culture studies; Glazer *et al*. [20] adopted the method to fabricate multi-stimuli responsive hydrogel cilia including MAC; and Chen *et al.* [21] used a micromoulding technique to fabricate MAC that were shown to be capable of mixing different fluids in a microfluidic device. In these cases, however, either the employed fabrication processes are time-consuming, or the fabricated MAC have relatively weak magnetic properties and hence cannot induce substantial flows in microfluidic devices.

The micro-moulding method we present in this paper enables to control and optimize the distribution of magnetic particles within the MAC, which dramatically improves the MAC's magnetic properties, actuation capabilities, and the flow propulsion capabilities. To demonstrate the versatility of our improved MAC, we integrated them in a microfluidic device. The results demonstrate that our MAC can form a fully integrated micro-pump ~~that acts as an artificial "mini-heart"~~.

2. Material and methods

2.1 Precursor material

The magnetic precursor material for creating MAC is a composite material of thermally curable polydimethylsiloxane (PDMS, Sylgard 184, Dow Corning, Base to Curing Agent weight ratio is 10:1) and magnetic microparticles, carbonyl iron powder (CIP, 99.5%, SIGMA-ALDRICH). The weight ratio between PDMS and CIP is 1:1 for all MAC except for MAC with concentrated magnetic particle distribution in the tips, for which the ratio is 5:1. The typical size of the magnetic particles is 5 µm in diameter according to Scanning Electron Microscope (SEM) images of these particles (see Appendix A for details).

We used the following process to prepare the magnetic precursor material (see Appendix B for more details about this process). First, magnetic particles (CIP) were sonicated in an Ethanol solution for 30 minutes at room temperature in an ultrasonic bath (Ultrasonic Cleaner, Branson 2510), and in the meantime the solution was stirred to prevent CIP from sinking. Then Ethanol was poured off and residual Ethanol was further removed using a vacuum system for 5 minutes. Afterwards, PDMS Base was added and the composite was mixed using a planetary centrifugal mixer (THINKY MIXER ARE-250CE, MIXING mode) with a revolution speed of 2000 rpm for 10 minutes, which was followed by sonication in the ultrasonic bath for 10 minutes at room temperature. Subsequently, PDMS Curing Agent was added to the mixture which was then mixed using the planetary centrifugal mixer in the same mode for 5 minutes. Finally, the mixture was mixed by hand for 10 minutes, and the PDMS-CIP mixture was ready for further use. The total preparation duration was around 1.5 hours which is only 1/4th of that of the method used by Pirmoradi *et al*. [22].

2.2 Fabrication of MAC

We initially fabricated MAC with a random magnetic particle distribution within cilia, termed standard MAC from now on, using a micro-moulding process consisting of six steps (shown in Fig. 1a): (1) A mould featured with micro-wells of diameter, depth and pitch of 50, 350, and 350 µm, respectively, was fabricated using standard photo-lithography with SU-8 2150 as photoresist (see Appendix C for details). (2) The prepared magnetic precursor material (PDMS-CIP mixture) was poured onto the mould, followed by a degassing procedure in order to pump out the trapped air gas within the micro-wells so that the micro-wells were filled with PDMS-CIP. (3) The top layer of PDMS-CIP was wiped away using cleanroom wipers. (4) Pure PDMS was poured onto the mould. After degassing the pure PDMS layer was defined to a thickness of around 100 µm by spin-coating at a rotating speed of 500 rpm for 50 seconds. The resulting pure PDMS layer would eventually form the transparent non-magnetic base substrate for the MAC. The non-magnetic nature of the substrate prevents the undesired magnetic interference between the substrate, the magnetic field, and the MAC, and its transparency enables optical observation from below the MAC substrate, e.g. allowing us to define the exact position of the actuating magnet. (5) The sample was left in an oven at 80 °C for 2 hours to cure the mixture. The reasons to do so are that an appropriate temperature such as 80 °C reduces the curing period of the precursor material and simultaneously prevents collapse of the MAC during and after release. (6) The cured pure PDMS layer with PDMS-CIP micropillars was peeled off the SU-8 mould. Finally, the MAC with the same geometry as the mould, namely a diameter, length and pitch of 50, 350, and 350 µm, respectively, were obtained, "standing" on a transparent PDMS base substrate.

With the intention to enhance the magnetic properties and the actuated motions of the MAC, we created two other kinds of MAC besides the standard MAC: MAC with a linearly aligned magnetic particle distribution (termed LAP MAC) and MAC with concentrated magnetic particles in the cilia tips (termed CP MAC). The alignment of magnetic particles into tight chains in the LAP MAC was expected to increase the cilia magnetization by creating an anisotropy of magnetic susceptibility (χ) not only due to cilia shape's anisotropy [19] but also due to a "particle arrangement anisotropy" (see section 3.1.2 for details). For the CP MAC we hypothesized that, on the one hand, the higher local particle concentration could enhance the magnetic forces, and on the other hand, the magnetic particle-free roots would improve the cilia's compliance so that the cilia would bend more easily.

Both the process to fabricate the LAP MAC and that of CP MAC are based on the process to fabricate the standard MAC. To fabricate the LAP MAC, during step 5, we applied a magnetic field to the sample by placing a permanent magnet with a size of

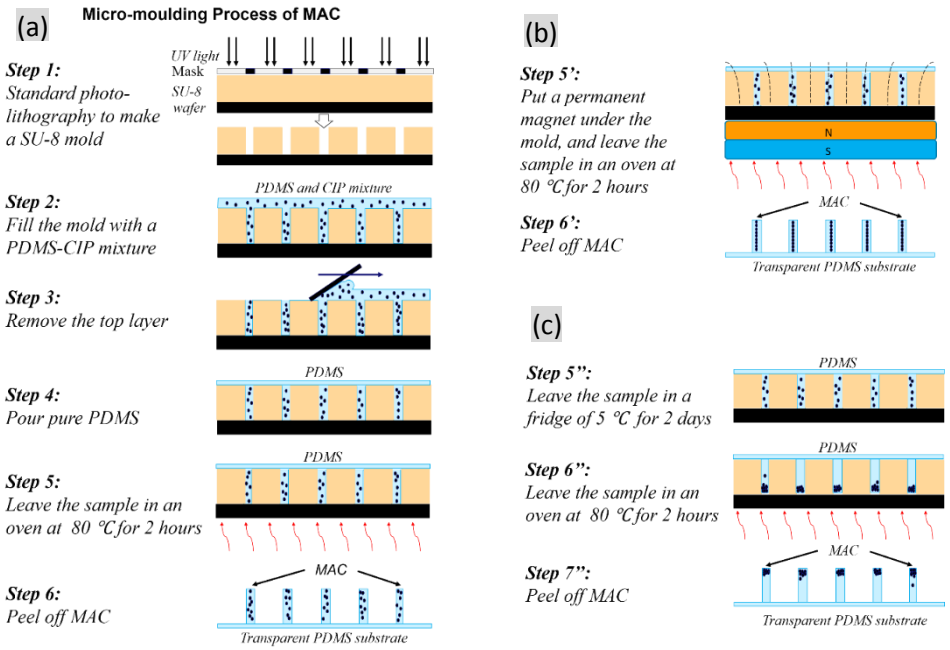

Fig. 1. Schematic of the micro-moulding process to fabricate MAC. (a) Standard process to fabricate MAC with a random magnetic particle distribution (standard MAC). (b) Last two steps to create MAC with a linearly aligned magnetic particle distribution (LAP MAC) employing a permanent magnet with a remnant flux density of 1.3 T to guide the distribution of magnetic particles within cilia. (c) Last three steps to make MAC with a concentrated particle distribution in cilia tips (CP MAC) using gravity induced sedimentation of magnetic particles. Illustrations are not to scale.

20x20x10 mm^3 and a remnant flux density of 1.3 T underneath the mould (Fig. 1b). The basic idea behind the creation of the LAP MAC is that magnetic particles tend to align themselves with the magnetic field forming a tight chain within a cilium [17]. The process to fabricate the CP MAC contains one step more than the process for fabricating the standard MAC, in which the sample is left in a fridge of 5 °C for 2 days (Fig. 1c Step 5"). Due to the density difference between PDMS and CIP (ρ_{CIP}:ρ_{PDMS} = 8:1), the magnetic particles tend to settle and deposit at the bottoms of the micro-wells in the mould which will eventually form the tips of the CP MAC. The low temperature applied during Step 5" prevents the PDMS from crosslinking too fast, so that the magnetic particles, within the 2 days duration of this process step, can completely settle without being held back by the crosslinking-induced increasing PDMS viscosity (see Appendix D for details).

2.3 Fabrication of microfluidic devices

The microfluidic devices were fabricated using soft-lithography which is actually a moulding process with pure PDMS as precursor material, and the master moulds were created using standard photo-lithography. Two kinds of PDMS microfluidic devices are used in this paper to characterize the capability of our MAC to generate substantial versatile flows. The first, shown in Fig. 2a, is a circular microfluidic device of a rectangular cross section with a constant channel width of 5 mm; such circular channels were used with different channel heights of 600, 700, 800 and 900 µm. The second device, shown in Fig. 2b, contains a branching channel network. There are 3 channel levels in the branching ~~blood vessel shaped~~ channel network with channel widths of 5 mm, 1.5 mm and 0.45 mm, respectively. The channel height of the branching channel network is 660 µm throughout.

In the fluid flow generation experiments, the MAC are positioned in the microfluidic devices at a specific location as shown in Fig. 2 in which the flow observation areas are also indicated. In all of the experiments reported in this paper, the ciliated area consisted of a 9 by 9 square array of 81 MAC.

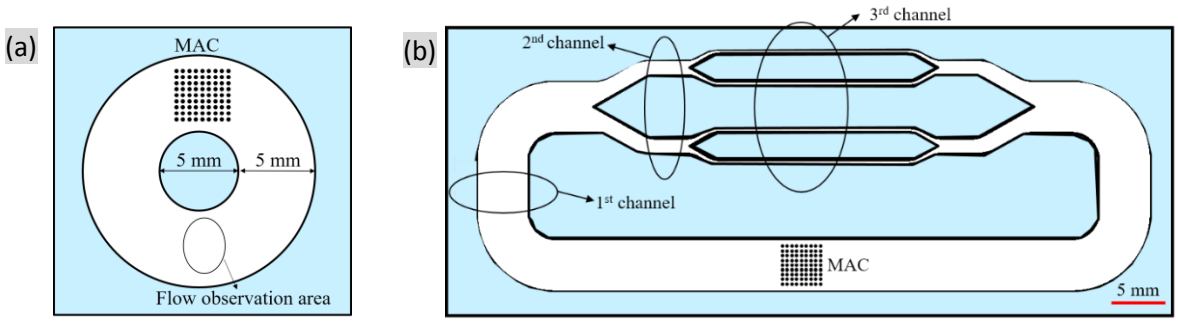

Fig. 2. Schematic of the microfluidic devices used in this paper to characterize the capability of our MAC to generate substantial and well controlled flows. (a) A circular microfluidic device with a constant channel width of 5 mm. The inner and outer cylindrical walls have a diameter of 5 and 15 mm, respectively. (b) A branching microfluidic channel network device featured with a three-levelled channel network, namely the 1st channel, 2nd channel and 3rd channel of width of 5 mm, 1.5 mm and 0.45 mm, respectively. The height of the channel network is 660 µm throughout.

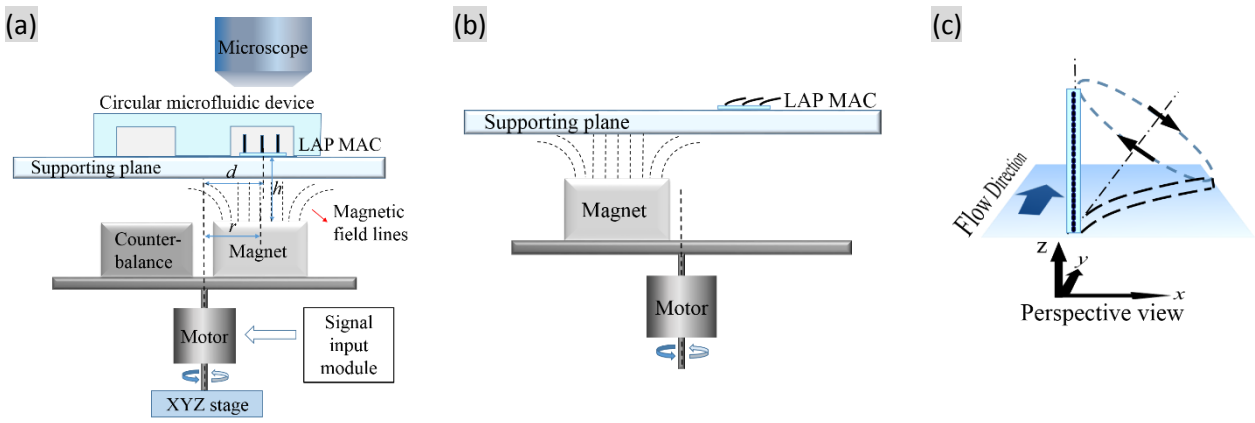

Fig. 3. Actuation scheme of the fabricated MAC. (a) Schematic of the actuation setup with cilia integrated in a circular microfluidic device on top. The rotation axis of the magnet is offset by a distance d with respect to the centre of the cilia chamber, and the magnet is placed at a distance r from the rotation axis. In the shown position, the cilia orientation is perpendicular to the substrate (effective stroke). (b) Schematic drawing of the bending cilia when the magnet rotates 180°. In this position, the cilia are bent (recovery stroke). (c) Schematic drawing of the cilia rotation in perspective view, with the generated flow direction indicated, which is in the direction of the effective stroke. Illustrations are not to scale.

2.4 Methods to measure the induced flow speed

2.4.1 Actuation setup

We used a homebuilt magnetic setup to actuate the MAC, as shown in Fig. 3a. The setup is comprised of a manual linear XYZ translational stage at the bottom part, an electric motor in the middle part, an offset counterbalanced magnet mounted on the motor and a safety box containing the supporting plane (a transparent glass plate of thickness of 1.5 mm) on top of which the MAC can be placed covered with a microfluidic device. The magnet, which has a geometry of 20×20×10 mm^3 with a remnant flux density of 1.3 T, is positioned at an offset with respect to its rotation axis which is also offset with respect to the center of the cilia chamber. The values for d, r, and h, which determine the location of the MAC with respect to the magnet (see Fig. 3a), were set to 6, 6.5 and 2 mm, respectively. This way, a time-dependent magnetic field is generated that actuates the cilia to perform a tilted conical motion (Fig. 3c) since the cilia tend to align their long axis with the magnetic field (Fig. 3a and b). During the tilted conical movement, the volume of fluid entrained by the cilium when its tip passes near the floor (recovery stroke, Fig. 3b) is less than that when its tip is farther away from the floor (effective stroke, Fig. 3a). This spatial asymmetry enables the cilia to produce a net flow in the same direction as the effective stroke in a complete beating cycle (Fig. 3c).

We used a high-speed camera to capture the top-view motion of the MAC and then analyzed the motion using an image analyzing software named ImageJ. Here we only observed the motion of the LAP MAC composed of 81 cilia (9 rows and 9 columns). The time-dependent magnetic field was obtained through the calculation of the relative position between the MAC and the actuating magnet, in combination with COMSOL simulations (see Appendix E for details).

2.4.2 Visualization of the generated flows

In order to study the capability of the LAP MAC to generate flows, a series of circular microfluidic devices and the branching channel network (see section 2.3 for details) were used. The flow was characterized at specific flow observation areas, indicated in Fig. 2. The liquid we used was deionized water and the flow speeds were visualized by seeding the fluid with 5 µm polystyrene tracer particles (micromod Partikeltechnologie GmbH). A high-speed camera connected to a stereo microscope was used to record the movement of the seeding particles by taking image sequences at a specific frame rate of 200 fps. The speeds of the tracer particles in the geometrical center of the microfluidic channels (where the flow speeds are the highest) were measured by a Manual Tracking analyses using ImageJ. Since the captured images give an integrated view of the tracer particles over the whole depth of the channel, only the maximum values were used to calculate the maximum flow velocities in order to eliminate the impact of particles not in the geometrical center of the channels. To estimate the precision of the measurements, standard deviations were calculated from the obtained velocities and these are indicated in the figures in sections 3.2.2 and 3.2.3.

The deionized water seeded with tracer particles was injected into microfluidic devices in the following way. First, the LAP MAC were temporarily modified to become hydrophilic through surface treatment using a plasma gun (Tantec HF SpotTEC) to prevent air from being trapped in the ciliated area. Second, a microfluidic device punched with one inlet and one outlet was placed on top of the LAP MAC with the LAP MAC located at the positions as shown in Fig. 2. Afterwards, deionized water seeded with tracer particles was injected into the microfluidic channel through the inlet. Last, both the inlet and the outlet were sealed with seal tabs (3M VHB) to prevent any interference from outside the system.

For evaluation of the pumping performance of the LAP MAC, the pressure difference and the volumetric flow rate generated by them in the microfluidic channels are two important parameters. We estimated these parameters by assuming that a fully developed Poiseuille flow is present throughout the device except in the ciliated region. Hence, based on the measured maximum flow speeds within the channels, we used the following equations [23][24] to calculate the corresponding pressure differences and volumetric flow rates generated by the LAP MAC:

$$\Delta P_f = \frac{\mu v_{xf}(0,\ 0) L \pi^3}{4h^2 \sum_{i=1,3,5,\ldots}^{\infty} (-1)^{\frac{i-1}{2}} \left[1 - \frac{1}{cosh\left(\frac{i\pi w}{2h}\right)}\right] \frac{1}{i^3}}, \quad for\ h < w \tag{1}$$

$$Q_f = \frac{\Delta P_f w h^3}{12 \mu L}\left[1 - \frac{192h}{\pi^5 w} \sum_{i=1,3,5,\ldots}^{\infty} \frac{tanh\left(\frac{i\pi w}{2h}\right)}{i^5}\right], \quad for\ h < w \tag{2}$$

where ΔP_f is the pressure difference over a channel section of length L, and Q_f is the corresponding volumetric flow rate, μ is the dynamic viscosity of the liquid, $v_{xf}(0, 0)$ is the measured translational flow speed in the geometrical center of the channels at actuation frequency f, and w and h are the cross-sectional dimensions of the rectangular channel. For the circular channels (Fig. 2a), the length L is defined as the total length of the circular channel minus the extent of the ciliated area. In case of the branching channel network (Fig. 2b), we applied equations (1) and (2) to each channel section separately. Subsequently, the overall pressure difference and volumetric flow rate over the complete network were obtained by appropriately adding the contributions in the various sections as explained in detail in Appendix H of the supplementary information. This means that, subject to the mentioned assumptions, the generated pressure difference estimated is that between the locations right before and after the ciliated area.

3 Results and discussion

3.1 Magnetic properties of the fabricated MAC

The magnetic properties of fabricated MAC were characterized through microscopy imaging (see Appendix I for details of the measurement), magnetization measurements (see Appendix J) and bending performance measurements (see Appendix B).

3.1.1 Magnetic particle distribution in the MAC

Fig. 4 shows the geometry and spatial arrangement of the fabricated MAC, and magnetic particle distributions within different kinds of these MAC. As shown in Fig. 4a, the moulded MAC have a well-defined cylindrical shape with a diameter of 50 µm, a length of 350 µm and a pitch distance of 350 µm. This statement is true for all three kinds of MAC according to SEM images although we only show one of these MAC. As shown in Fig. 4b, within the standard MAC, the magnetic particles are randomly distributed; i.e. the image shows random regions of high and low particle concentrations. On the other hand, as shown in Fig. 4c (especially in the cross-sectional view), within the LAP MAC, magnetic particles are closely connected to each other forming a chain in every single cilium, as a result of the applied magnetic field during cilia fabrication. It is important to stress that in the LAP MAC the magnetic particles are constrained in the cilia and rarely protrude into the pure PDMS base substrate. This could be the result of magnetic attraction of the magnetic particles by the permanent magnet, which attracts the particle downwards to the tips of the cilia (see Fig. 1b). This attraction effect is probably also the reason why the LAP MAC have a magnetic particle-free region close to their roots, as clearly visible in Fig. 4c; this particle-free region may create additional cilia flexibility. Fig. 4d shows that in the majority of the CP MAC, magnetic particles are concentrated at the cilia tips within a range of 1/5th of the total length of the cilia. This concentrated magnetic particle distribution possibly generates focused magnetic forces at the cilia tips in an applied magnetic field, and at the same time renders the magnetic particle-free pure PDMS roots in the cilia, contributing to an enhanced cilia flexibility. The different magnetic particle distributions may result in different magnetic properties for the three different types of MAC.

3.1.2 Magnetization of the MAC

Fig. 5 shows the measured magnetization of all three types of MAC from SQUID measurements. Several observations can be made. **First**, it is clear that at a specific magnetic field both the standard MAC and the LAP MAC have a larger susceptibility (χ) when the magnetic field is applied parallel to the long axis of the cilia, confirming that the cilia shape's anisotropy leads to an

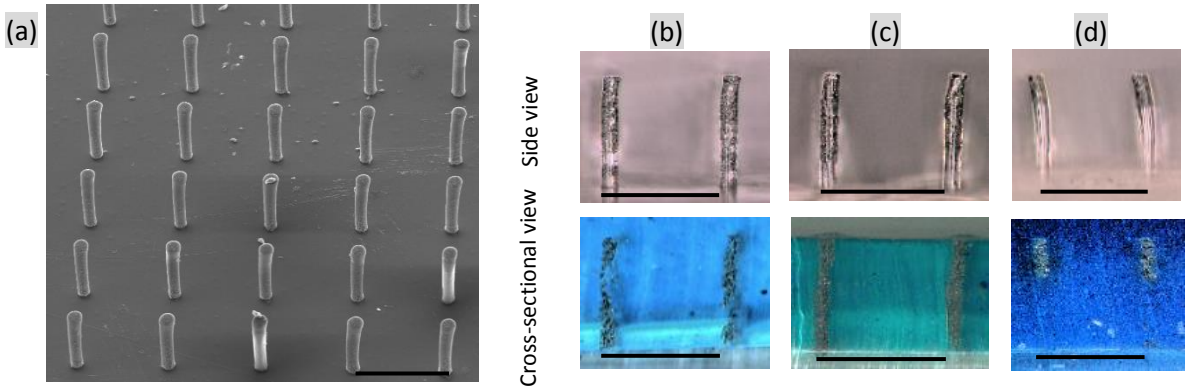

Fig. 4. Microscopy images of the fabricated MAC: (a) SEM image of the MAC with a diameter, length and pitch of 50, 350, and 350 µm, respectively, taken at a 30° angle. Optical microscopy images of (b) the standard MAC, (c) the LAP MAC, and (d) the CP MAC in both side view and cross-sectional view (see Appendix I for details regarding the imaging methods). All scale bars are 350 µm.

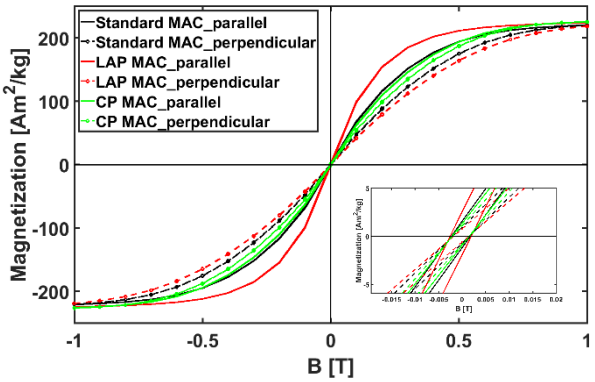

Fig. 5. Symmetric hysteresis loops showing magnetization of the three types of MAC as a function of applied magnetic field with the application direction parallel and perpendicular to the long axis of cilia, respectively. The insert is the partial enlargement near the origin to show the remnant magnetization and coercive field.

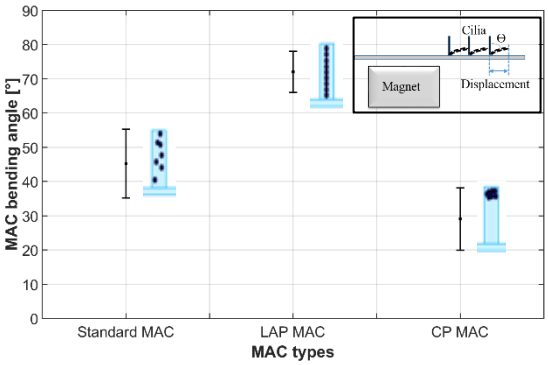

Fig. 6. Calculated average bending angles of three types of MAC. The error bars are the standard deviations of the calculated bending angles of 81 cilia for each sample. The insert shows the schematic of the measurement for MAC tips' displacement and the definition of the corresponding bending angle (see Appendix B for details).

anisotropy of χ, i.e. a larger χ in the long axis of the cilia. This was already observed by Khademolhosseini and Chiao [19] for random magnetic particle distributions. Although the anisotropy of χ happens for the CP MAC too, it is very low. This is probably caused by the low aspect ratio of the magnetic tip so that the distribution of magnetic particles in the CP MAC has a similar length in the direction along the long axis of the cilia (70 μm = 1/5 of the CP MAC length) as in the direction perpendicular to the long axis of the cilia (50 μm = the diameter of the CP MAC), which leads to a low anisotropy of χ. **Second**, at any specific magnetic field the difference between the magnetization obtained for the parallel and perpendicular magnetic field is larger for the LAP MAC than for the standard MAC. This is caused by the more anisotropic distribution of magnetic particles in the LAP MAC (see Fig. 4c). The anisotropy of χ is enhanced for the LAP MAC, since the particle alignment results in a "particle arrangement anisotropy" in addition to the "shape anisotropy". **Third**, when the magnetic field is applied parallel to the long axis of the cilia, the LAP MAC have a significantly larger χ than the standard MAC over the full range of the applied magnetic field, which is also a result of the enhanced anisotropy of χ. This larger χ may result in a larger bending angle for the LAP MAC. The largest magnetization difference between the two MAC types is 33% at an applied field around 0.2 T which is within the range of the magnetic field experienced by the MAC during actuation using our homebuilt actuation setup (see Fig. E.3a in Appendix E). **Last**, the CP MAC have the lowest magnetization at a specific applied magnetic field, which most probably is caused by the lowest anisotropy of the magnetic particle distribution. To summarize, the different magnetic particle distributions within the MAC result in differences in χ of the MAC, which is expected to lead to differences in the actuation of MAC in an applied magnetic field.

3.1.3 Bending performance of the MAC

The extent of the bending of the MAC under the influence of a static external magnetic field was measured using the method described in Appendix B, where the bending angle Θ (as indicated in the insert of Fig. 6) was calculated from the tips' projected displacement with the assumption that cilia are rigid rods that only bend at the anchor points. Thus,

$$\sin\Theta = \frac{tips'\ displacement}{the\ length\ of\ cilia} \tag{3}$$

The calculated bending angles are shown in Fig. 6. It is clear that due to differences in the specific particle distributions between individual MAC, the bending angle shows substantial differences. The average bending angle of the standard MAC is 45°, while the average bending angle of the LAP MAC is 72°, which is 60% larger! This dramatic increase of bending angle can be attributed to the enhanced χ of the LAP MAC as shown in Fig. 5. The average bending angle of the CP MAC is 29°, the smallest of the three kinds of MAC we produced. This could be due to the fact that the mass of the magnetic particles in the CP MAC is only 1/5th of that in the other two types of MAC (and hence a smaller magnetic moment, since the magnetic moment is the product of the mass of magnetic particles and the magnetization), and that the decrease in stiffness does not compensate the decrease of magnetic forces, which eventually leads to a decreased bending angle. Note that, the standard deviation of the bending angle of the LAP MAC is the smallest, which means the bending performance of the LAP MAC is the most uniform.

We made a theoretical comparison of the expected bending performance of the fabricated MAC by estimating the magnetic forces applied on the MAC (see Appendix F for details). The results confirm that the LAP MAC are subjected to the largest magnetic forces, while the CP MAC are subjected to the smallest magnetic forces, which explains why the LAP MAC bend the most.

Because the LAP MAC have the largest bending angle and the most uniform performance, we selected these cilia to perform the fluid flow experiments. There is another reason for choosing the LAP MAC, namely during actuation, there turned out to be a strong interaction between cilia for both the standard MAC and the CP MAC, but not for the LAP MAC. The interaction resulted in attraction and adherence between neighboring cilia tips as shown in Appendix G. This was probably caused by the arbitrary direction of their magnetic moment, which resulted in arbitrary magnetic forces.

3.2 Actuation of the LAP MAC and flow generation

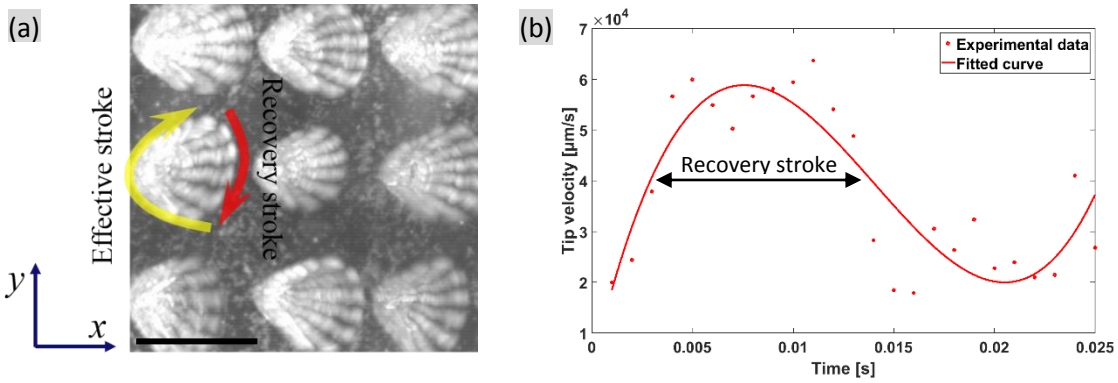

Fig. 7. (a) Top-view image of the motion of the rotating LAP MAC in air showing the tilted cone rotation, composed of 25 frames in one actuation cycle at 40 Hz. The scale bar is 350 μm. (b) The projected MAC tip velocity during one actuation cycle at an actuation frequency of 40 Hz in air. Experimental data means the data from the direct measurements by doing Manual Tracking of the cilia tip using ImageJ; and the fitted curve means the fitted velocity from the experimental data using a third degree polynomial curve.

3.2.1 The motion of the LAP MAC

The motion of the LAP MAC in air was recorded by the high-speed camera at 1000 fps when the actuating magnet was rotating at a frequency of 40 Hz (the limit of our actuation setup). A video of the cilia motion can be found in the supplementary material I. Through analyzing the high-speed images using ImageJ, we obtained the projected cilia and cilia tip trajectories pictured in Fig. 7a, which shows that our LAP MAC approximately perform a tilted conical motion containing two strokes in one rotating cycle – the effective stroke and the recovery stroke. From the analysis of the cilia motion, we also extracted the projected instantaneous velocity of the cilia tip during one actuation cycle at the rotation frequency of 40 Hz in air (shown in Fig. 7b). We can see that the LAP MAC move faster during the recovery stroke than during the effective stroke. For the explanation, please refer to Appendix E. This explanation also confirms that our MAC follow the magnetic field instantaneously.

For the generation of a net flow, on the other hand, it can be advantageous if the MAC move faster during the effective stroke than during the recovery stroke, at least if inertial effects play a role. To confirm this in our particular actuation, we can calculate the local Reynolds number, defined by $Re = \rho v L/\eta$, in which ρ is the density of the fluid (in our case water), η is the dynamic viscosity of the fluid (0.89 cP in our case), L is the characteristic length for which we take the cilia length (350 μm in our experiments). Finally v is the average speed of the cilia tips at the rotation frequency in our experiments at 40 Hz (around 0.04 m/s, as calculated from Fig. 7b). Therefore the local Reynolds number Re is around 15 > 1, and indeed inertial effects are expected to play a role [25]. To be able to control the time-dependency of the magnetic field, an electromagnetic setup could be a more versatile alternative to the rotating permanent magnet we used. Such optimization is, however, beyond the scope of the present work.

3.2.2 Flows in the circular chips

Fig. 8 shows the calculated flow parameters as a function of actuation frequency in circular microfluidic devices with varying channel height. A video of the cilia motion and corresponding generated fluid flows in a circular channel of height 900 μm can be found in the supplementary material III. Several observations can be made from the results. First, as shown in Fig. 8a the flow speed increases with actuation frequency as expected. At small frequencies, the flow speed is proportional with frequency and at higher frequencies the dependency is less than linear. Notably, the less-than-linear relationship is more obvious for channels of smaller height of 700 and 600 μm; in the latter case the flow speed even becomes frequency-independent when the actuation frequency is higher than 35 Hz. Second, the flow speed at a specific actuation frequency is larger in a higher channel. Third, Fig. 8b shows that the estimated pressure drop generated by the LAP MAC is the same for all circular channel heights at actuation frequency up to about 15 Hz. For larger actuation frequencies, the results for different channel heights deviate slightly. Finally, the volumetric flow rate shown in Fig. 8c shows a similar trend as the flow speed.

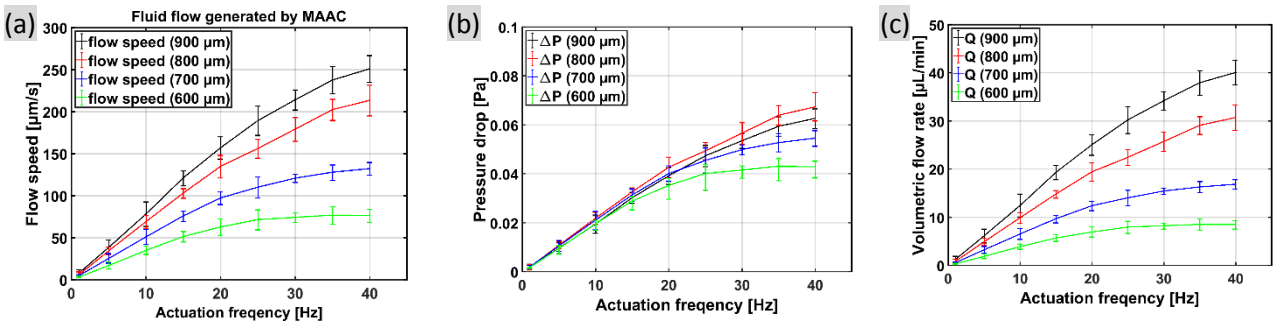

Fig. 8. (a) Flow speed of water observed from the circular channels for different channel heights and as a function of actuation frequency. (b) Pressure difference and (c) corresponding volumetric flow rate generated by the LAP MAC in circular channels calculated using the Eq. 1 and Eq. 2. The error bars are the standard deviations of the obtained data.

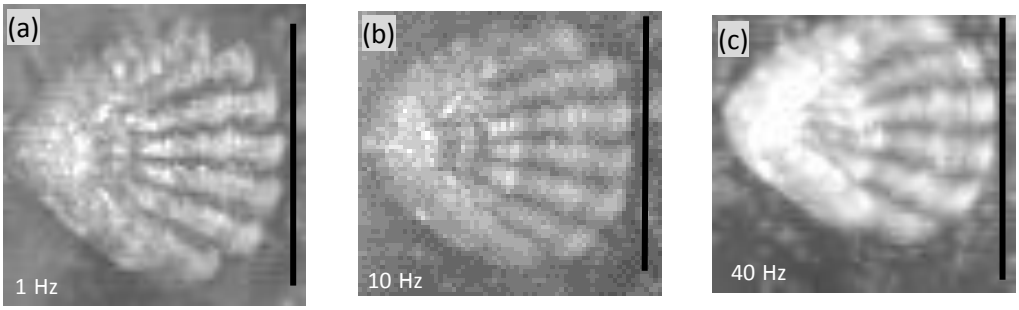

Fig. 9. Top-view image of the motion of the rotating LAP MAC in a 600 µm channel at an actuation frequency of (a) 1 Hz, (b) 10 Hz, and (c) 40 Hz taken with a high-speed camera. At higher frequencies, the extent of the motion is reduced because of increasing viscous drag. All scale bars are 350 µm.

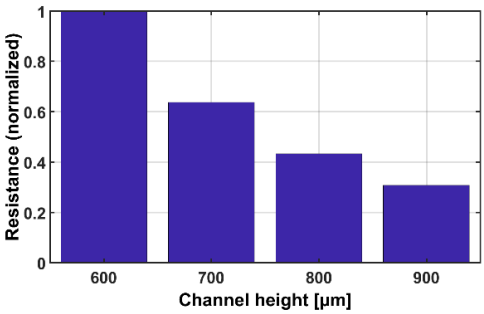

Fig. 10. Resistance in circular channels normalized with the resistance in the 600 µm calculated from Eq. (4).

The dependency of the flow speed on the actuation frequency can be explained as follows. At actuation frequencies lower than 15 Hz (Re < 5, and the inertial effect of the liquid is not important), the LAP MAC perfectly follow the magnetic field in all cases such that in each revolution cycle the LAP MAC transport the same amount of liquid [13][17], and therefore the flow speed scales linearly with frequency. For higher frequencies, the less-than-linear relationship can be explained as follows. First, the cilia experience an increased hydrodynamic drag as the rotation frequency increases, which causes the motion of the cilia to diminish as shown in Fig. 9. Hence the net flow generated by the cilia in one rotating cycle decreases, and the relationship between the flow speed and the actuation frequency becomes less than linear. When the frequency is further increased, this diminished cilia motion will at some point even lead to a reduction in the fluid flow generated by the cilia per unit time, and the induced flow speed will decrease with increasing frequency [16], [17]. We expect that, when the actuation frequency would be further increased beyond 40 Hz, the flow speeds in 700, 800 and 900 µm channels will increase further before they reach a point after which they will decrease, and that the flow speed in the 600 µm channel will start to decrease because it seems like the speed has already reached the threshold. We believe that if the magnetic property of the LAP MAC could be further improved and/or a permanent magnet with a stronger magnetic field is employed, the threshold would be postponed to a higher actuation frequency and thus a higher flow speed could be generated by the LAP MAC. Such optimization is still ongoing. Second, in the ciliated area complex flow patterns are actually generated by the rotating cilia, resulting in local backflow and recirculation (see electronic supplementary material IV). These effects can be dependent on actuation frequency, and on channel geometry, i.e. channel height in our case. Third, the non-linear relationship could be partially due to the fact that our cilia move faster during the recovery stroke, and that the local Reynolds number is larger than 1 for actuation frequencies beyond 3 Hz when the inertial effect begin to play a role (see the discussion at the end of section 3.2.1).

We find almost the same pressure drop for different channel heights, at least of the rotation frequency of the cilia is smaller than 15 Hz (see Fig. 8(b)). Therefore, at equal power input (basically determined by the motor driving the rotating magnet), the artificial cilia appear to deliver the same pressure head irrespective of channel height. For larger frequencies, the effects mentioned above, in particular increased drag and backflow and recirculation, may act as additional power dissipation sources that cause the delivered pressure head to deviate for different channel heights.

The increase of volumetric flow rate for higher channels can be easily understood by considering the hydraulic resistance of the channels, defined by $R=\Delta P_f/Q_f$. According to Eq. 2, R can be derived as following:

$$R = \frac{12\mu L}{wh^3\left[1-\frac{192h}{\pi^5 w}\sum_{i=1,3,5,\ldots}^{\infty}\frac{tanh\left(\frac{i\pi w}{2h}\right)}{i^5}\right]}, for\ h < w \qquad (4)$$

For the various circular channels, R is plotted in Fig. 10. It is clear that the resistance of a higher channel is smaller. As Q_f is inversely proportional to R, the smaller R results in a larger Q_f in a higher channel at equal ΔP_f.

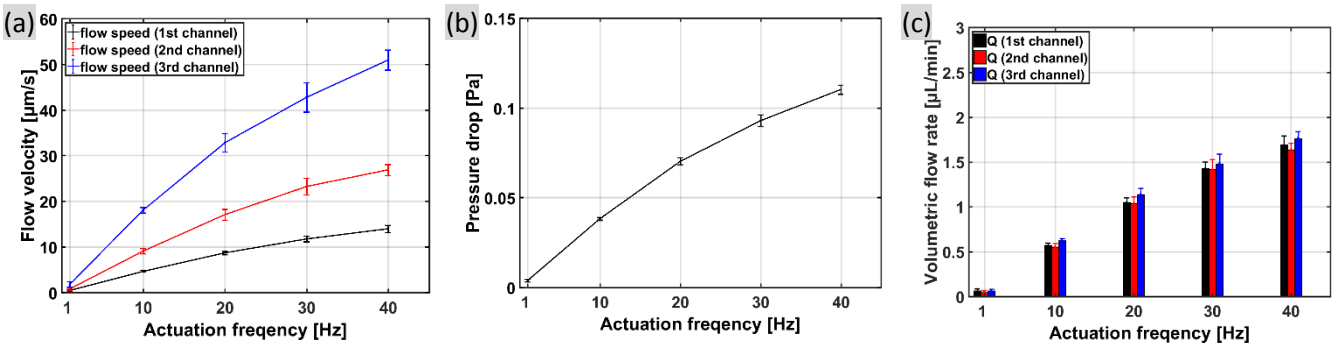

Fig. 11. (a) Flow speed generated by the LAP MAC in the branching channel network as a function of actuation frequency. (b) Corresponding pressure difference and (c) volumetric flow rate calculated using the Eq. 1 and Eq. 2, respectively (see Appendix H for details). The error bars are the standard deviations of the obtained data.

Finally, as shown in Fig. 8b and Fig. 8c, our LAP MAC are able to generate a maximum pressure difference of 0.065 Pa and a maximum volumetric flow rate of 40 μL/min in a 900 μm circular channel, which is competitive with the performance of most of the electro-hydrodynamic and electroosmotic pumping methods reviewed by Laser and Santiago [26]. See Appendix H for a more detailed comparison.

3.2.3 Flows in the branching channel network

As already shown in 3.2.2, our MAC are capable of generating substantial flows in circular microfluidic channels, and we designed a more complex channel network, a branching channel network as described in section 2.3 and shown in Fig. 2b, to demonstrate the cilia-generated flow in more complex microfluidic applications. We carried out the same flow measurements as described in section 3.2.2 using exactly the same LAP MAC, and the results are shown in Fig. 11. As shown in Fig. 11c, our LAP MAC can generate a volumetric flow rate of up to 1.7 μL/min in the branching channel network, which corresponds to maximum flow speeds of 14, 27 and 51 μm/s in various parts of the channel network (Fig. 11a). Here we expect the flow speed will further increase with actuation frequency before it reaches a threshold when the actuation frequency is increased up to a critical value. However 40 Hz is the limit of our magnetic actuation setup, and the threshold cannot be reached.

As shown in Fig. 11b, the estimated pressure difference generated by our LAP MAC in the branching channel network is up to 0.11 Pa at 40 Hz, which is approximately triple of that generated in the circular channels of approximately the same height (600 μm). From Fig. 8b, we concluded that the pressure difference generated by the LAP MAC is the same for each circular channel height, at least for frequencies smaller than 15 Hz. This seems to be in contradiction with the fact that the pressure drop in the branching channel network is different from that in the circular channel, even though the MAC configuration and the driving magnetic field are the same. An explanation for the difference might be that, in estimating the pressure drop, we assume that a fully developed Poiseuille flow exists within the whole device (except for the MAC area); this assumption is clearly not fully valid for the branching channel network, especially at the locations of the branching, and this may lead to errors in the estimated pressure drop.

As shown by comparing Fig. 11c and Fig. 8c, the estimated volumetric flow rate in the branching channel network is only around 1/5th of that in the 600 μm circular channel. The main reason for this is that the resistance R of the branching channel network is 13 times as large as that of the 600 μm circular channel (see appendix H for details of the computation of the resistance), thus, according to $\Delta P_f = RQ_f$, the volumetric flow rate in the branching channel network is 3/13th≈1/5th of that in the 600 μm circular channel, and therefore the measured pressure drop – flow rate combinations are indeed consistent. A video of the flows in different parts of the branching channel network can be found in the supplementary material V.

3.2.4 Versatile fluid flows

Notably, in both types of microfluidic devices, versatile fluid flows can be generated by tuning the motion of the actuating magnet as our LAP MAC follow the magnetic field swiftly as illustrated in Appendix E. For example, when we change the rotating direction of the magnet, the rotating direction of the LAP MAC also changes, which creates **direction-reversible flow**. Fig. 12a shows one cycle of the generated water flow profile of the direction-reversible flow in the 900 μm circular channel when the input of the actuation frequency is as follows:

$$f_{in1} = \begin{cases} 40\sin\pi t, & 0 \le t \le 0.05 \\ 40, & 0.05 < t < \dfrac{T_1 - 1}{2} \\ 40\sin\pi\left(t - \dfrac{T_1}{2} + 1\right), & \dfrac{T_1 - 1}{2} \le t \le \dfrac{T_1 + 1}{2} \\ -40, & \dfrac{T_1 + 1}{2} < t < T_1 - 0.5 \\ 40\sin\pi(t - T_1 + 2), & T_1 - 0.5 \le t \le T_1 \end{cases}$$

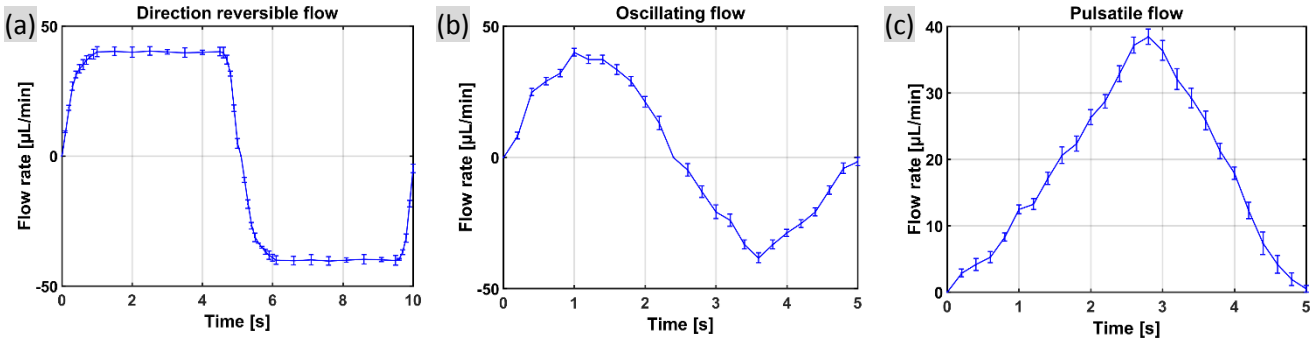

Fig. 12. Versatile water flows generated by the LAP MAC. (a) Direction-reversible flow achieved by altering the rotating direction of the actuating magnet. (b) Oscillating flow created by periodically altering the rotating direction of the actuating magnet. (c) Pulsatile flow generated by periodically altering the rotation frequency of the actuating magnet.

where T_1 is the time period of the actuation, and here we use T_1=10 s. **Oscillating flow** can also be generated by altering the rotation direction of the magnet periodically. One cycle of the generated flow profile in the 900 μm circular channel is depicted in Fig. 12b when the input of the actuation frequency is given like this:

$$f_{in2} = 40 \sin \frac{2\pi t}{T_2}$$

where $T_2 = 5$ s is the time period of the actuation. Another interesting example is the generation of **pulsatile flow** by periodically altering the rotation frequency of the actuating magnet. One cycle of the generated flow profile in the 900 μm circular channel is shown in Fig. 12c given the input of the actuation frequency is:

$$f_{in3} = 20 \sin \frac{2\pi(t - \frac{T_3}{4})}{T_3} + 20$$

where $T_3 = 5s$ is the time period of the actuation.

Several videos of the cilia motion and corresponding versatile flows in the 900 μm circular channel can be found in the supplementary material VI, VII and VIII. It is necessary to stress here that the flow profile of the versatile flows can be easily tuned by changing the inputs. For example, the duration of the flow profile and the peak flow speed can be adjusted by modifying the time period of the actuation and the amplitude of the actuation frequency accordingly. In that way, the flow generated by our LAP MAC can mimic physiological flow profiles such as actual blood flow in our vessels [27], especially when a more versatile control over the magnetic field is realized (e.g. using an electromagnet).

It is important to stress here that we did not observe any breaking or rupture of the MAC during long-run (2 weeks) experiments, which clearly proves that our MAC are mechanically robust.

4. Conclusions

In this paper, geometrically well-defined magnetic artificial cilia (MAC) on a transparent, non-magnetic base substrate were fabricated using a facile, highly reproducible micro-moulding process. The distribution of magnetic particles within the cilia can be controlled in this process so that MAC with a random magnetic particle distribution (standard MAC), MAC with a linearly aligned magnetic particle distribution (LAP MAC), and MAC with a concentrated magnetic particle distribution in the cilia tips (CP MAC) can be created. A uniform precursor material for creating the MAC was prepared using an efficient process by combining mechanical and ultrasonic mixing. Magnetization measurements in combination with characterization of the cilia deformation in a static magnetic field confirm that the LAP MAC have superior magnetic properties and corresponding actuation capabilities, while the CP MAC turned out to have the weakest magnetic response due to the small magnetic moment and the absence of a substantial magnetic gradient during actuation in a quasi-uniform field. Measurements of the speed of the cilia motion in conjunction with the calculation and COMSOL simulations of the time-dependent magnetic field that the cilia experienced during actuation, verify that our LAP MAC follow the magnetic field instantaneously, when actuated in air.

Fluid flow generation experiments show that the LAP MAC are able to generate water flow speeds of up to 260 μm/s in a circular channel of a rectangular cross section with a height of 900 μm and a width of 5 mm, which corresponds to a pressure difference of 0.65 Pa and a volumetric flow rate of 40 μL/min. Importantly, we found that the LAP MAC generate a constant pressure difference in the same type of circular microfluidic devices, independent of the channel's geometry, as long as the cilia motion is not diminished by the hydrodynamic drag caused by the liquid. In a more complex chip with a branching channel network, the LAP MAC are also capable of generating substantial circulatory flow. Our LAP MAC outperform most of the previously published artificial cilia in terms of actuation properties and fluid flow generation capabilities (see the supplementary Appendix H for a detailed comparison between our LAP MAC and some of previously published artificial cilia). Specifically, only the electrostatically actuated cilia reported in [3] generate higher fluid flow velocity (i.e. 600 μm/s), but these artificial cilia require a tedious manufacture process, and are not compatible with biological applications. Compared to other magnetic artificial cilia, our LAP MAC's generated flow speed is at least twice as large (e.g. as that in [17]) but offer more flexibility in design and easier

fabrication. In addition, the performance of our LAP MAC is competitive with that of most of the electro-hydrodynamic and electroosmotic pumping methods reviewed by Laser and Santiago [26], but our method does not require integration of electrodes (see Appendix H).

Importantly, our LAP MAC are capable of generating well-controlled flows because the LAP MAC have a high χ and follow the magnetic field swiftly. For example direction-reversible flows, oscillating flows and pulsatile flows can be generated by tuning the motion of the actuating magnet, which are out of reach when using conventional pumps such as a commercial syringe pump system. Compared to other pumping methods, our on-chip/ in-situ cilia-based micro-pump does not need tubing or electric connections, which, therefore, allows for the construction of a more compact system, reducing the usage of reagents by reducing dead volumes, avoiding undesirable electrical effects, and accommodating a wide range of fluids. This novel micropump could find applications in general microfluidic chips in which circulatory flows are required. One particular application is "organ-on-a-chip" in which microtissues representing human organs are cultured, connected by microchannels mimicking blood vessels [28]. Our artificial versatile integrated micropump could provide a compact and integrated solution to create physiologically relevant flows in these microchannels.

5. Acknowledgement

This research is funded by the Chinese Scholarship Council. We would like to thank Erwin Dekkers and Roel Brouwers for constructing the magnetic actuation setup, and Marc van Maris for helping in taking SEM images of MAC.

References

[1] G. M. Whitesides, "The origins and the future of microfluidics.," *Nature*, vol. 442, no. 7101, pp. 368–73, 2006.

[2] J. den Toonder and P. R. Onck, (eds) (2013), *Artificial Cilia*, Cambridge: RSC Publishing; ISBN: 978-1-84973-597-1.

[3] J. den Toonder, F. Bos, D. Broer, L. Filippini, M. Gillies, J. de Goede, T. Mol, M. Reijme, W. Talen, H. Wilderbeek, V. Khatavkar, and P. Anderson, "Artificial cilia for active micro-fluidic mixing.," *Lab Chip*, vol. 8, no. 4, pp. 533–41, 2008.

[4] S. Khaderi, C. Craus, J. Hussong, and N. Schorr, "Magnetically-actuated artificial cilia for microfluidic propulsion," *Lab Chip*, pp. 2002–2010, 2011.

[5] S. Khaderi, J. Hussong, J. Westerweel, J. Den Toonder, and P. Onck, "Fluid propulsion using magnetically-actuated artificial cilia – experiments and simulations," *RSC Adv.*, vol. 3, no. 31, p. 12735, 2013.

[6] A. R. Shields, B. L. Fiser, B. a Evans, M. R. Falvo, S. Washburn, and R. Superfine, "Biomimetic cilia arrays generate simultaneous pumping and mixing regimes.," *Proc. Natl. Acad. Sci. U. S. A.*, vol. 107, no. 36, pp. 15670–15675, 2010.

[7] C. L. van Oosten, C. W. M. Bastiaansen, and D. J. Broer, "Printed artificial cilia from liquid-crystal network actuators modularly driven by light.," *Nat. Mater.*, vol. 8, no. 8, pp. 677–82, Aug. 2009.

[8] L. D. Zarzar, P. Kim, and J. Aizenberg, "Bio-inspired design of submerged hydrogel-actuated polymer microstructures operating in response to pH," *Adv. Mater.*, vol. 23, no. 12, pp. 1–5, 2011.

[9] K. Oh, B. Smith, S. Devasia, J. J. Riley, and J. H. Chung, "Characterization of mixing performance for bio-mimetic silicone cilia," *Microfluid. Nanofluidics*, vol. 9, no. 4–5, pp. 645–655, 2010.

[10] K. Oh, J. Chung, S. Devasia, and J. J. Riley, "Bio-mimetic silicone cilia for microfluidic manipulation," *Lab Chip*, vol. 9, pp. 1561–1566, 2009.

[11] B. Gorissen, M. de Volder, and D. Reynaerts, "Pneumatically-actuated artificial cilia array for biomimetic fluid propulsion," *Lab Chip*, vol. 15, no. 22, pp. 4348–4355, 2015.

[12] B. A. Evans, A. R. Shields, R. L. Carroll, S. Washburn, M. R. Falvo, and R. Superfine, "Magnetically actuated nanorod arrays as biomimetic cilia," *Nano Lett.*, vol. 7, no. 5, pp. 1428–1434, 2007.

[13] M. T. Downton and H. Stark, "Beating kinematics of magnetically actuated cilia," *EPL (Europhysics Lett.*, vol. 85, no. February, p. 44002, 2009.

[14] M. Vilfan, A. Potočnik, B. Kavčič, N. Osterman, I. Poberaj, D. Babič, T. C. Lubensky, A. Potocnik, B. Kavcicb, N. Ostermanac, I. Poberajc, A. Vilfana, D. Babicc, and M. Vilfan, "Self-assembled cilia artificial," vol. i, 2015.

[15] A. Babataheri, M. Roper, M. Fermigier, and O. Du Roure, "Tethered fleximags as artificial cilia," *J. Fluid Mech.*, vol. 678, no. 2011, pp. 5–13, 2011.

[16] Y. Wang, Y. Gao, H. Wyss, P. Anderson, and J. den Toonder, "Out of the cleanroom, self-assembled magnetic artificial cilia.," *Lab Chip*, vol. 13, no. 17, pp. 3360–6, 2013.

[17] Y. Wang, Y. Gao, H. M. Wyss, P. D. Anderson, and J. M. J. den Toonder, "Artificial cilia fabricated using magnetic fiber drawing generate substantial fluid flow," *Microfluid. Nanofluidics*, vol. 18, no. 2, pp. 167–174, 2014.

[18] Y. Wang, J. den Toonder, R. Cardinaels, and P. Anderson, "A continuous roll-pulling approach for the fabrication of magnetic artificial cilia with microfluidic pumping capability," *Lab Chip*, vol. 16, pp. 2277–2286, 2016.

[19] F. Khademolhosseini and M. Chiao, "Fabrication and patterning of magnetic polymer micropillar structures using a dry-nanoparticle embedding technique," *J. Microelectromechanical Syst.*, vol. 22, no. 1, pp. 131–139, 2013.

[20] P. J. Glazer, J. Leuven, H. An, S. G. Lemay, and E. Mendes, "Multi-Stimuli Responsive Hydrogel Cilia," *Advanced functional materials*, vol. 23, no. 23. pp. 2964–2970, 2013.

[21] C.-Y. Chen, C.-Y. Chen, C.-Y. Lin, and Y.-T. Hu, "Magnetically actuated artificial cilia for optimum mixing performance in

microfluidics.," *Lab Chip*, vol. 13, pp. 2834–9, 2013.
[22] F. Pirmoradi, L. Cheng, and M. Chiao, "A magnetic poly(dimethylesiloxane) composite membrane incorporated with uniformly dispersed, coated iron oxide nanoparticles," *J. Micromech. Microeng*, vol. 20, pp. 15032–7, 2010.
[23] F. M. White, *Viscous Fluid Flow*, McGraw-Hill, 2006.
[24] H. Bruus, *Theoretical Microfluidics*, Oxford, 2008.
[25] M. G. H. M. Baltussen, P. D. Anderson, F. Bos, and J. M. J. den Toonder, "Inertial flow effects in a micro-mixer based on artificial cilia," *Lab Chip*, vol. 9, no. 16, pp. 2326–2331, 2009.
[26] D. J. Laser and J. G. Santiago, "A review of micropumps," *Journal of Micromechanics and Microengineering*, vol. 14, no. 6, R35–R64, 2004.
[27] J. J. Smolich, K. R. Kenna, and J. P. Mynard, "Retrograde lower body arterial reservoir discharge underlies rapid reversal of ductus arteriosus shunting after early cord clamping at birth in preterm lambs," pp. 399–407, 2016.
[28] D. J. Beebe, D. E. Ingber, and J. den Toonder, "Organs on Chips 2013," Lab Chip, vol. 13, pp. 3447–3448, 2013.